ACS OMEGA

http://pubs.acs.org/journal/acsodf

Article

Mutational Insight into Allosteric Regulation of Kir Channel Activity

Maryam Yekefallah, Carver A. Rasberry, Evan J. van Aalst, Holley P. Browning, Reza Amani, Derek B. Versteeg, and Benjamin J. Wylie*

Cite This: *ACS Omega* 2022, 7, 43621−43634

Read Online

ACCESS | Metrics & More | Article Recommendations | Supporting Information

ABSTRACT: Potassium (K^+) channels are regulated in part by allosteric communication between the helical bundle crossing, or inner gate, and the selectivity filter, or outer gate. This network is triggered by gating stimuli. In concert, there is an allosteric network which is a conjugated set of interactions which correlate long-range structural rearrangements necessary for channel function. Inward-rectifier K^+ (Kir) channels favor inward K^+ conductance, are ligand-gated, and help establish resting membrane potentials. KirBac1.1 is a bacterial Kir (KirBac) channel homologous to human Kir (hKir) channels. Additionally, KirBac1.1 is gated by the anionic phospholipid ligand phosphatidylglycerol (PG). In this study, we use site-directed mutagenesis to investigate residues involved in the KirBac1.1 gating mechanism and allosteric network we previously proposed using detailed solid-state NMR (SSNMR) measurements. Using fluorescence-based K^+ and sodium (Na^+) flux assays, we identified channel mutants with impaired function that do not alter selectivity of the channel. In tandem, we performed coarse grain molecular dynamics simulations, observing changes in PG-KirBac1.1 interactions correlated with mutant channel activity and contacts between the two transmembrane helices and pore helix tied to this behavior. Lipid affinity is closely tied to the proximity of two tryptophan residues on neighboring subunits which lure anionic lipids to a cationic pocket formed by a cluster of arginine residues. Thus, these simulations establish a structural and functional basis for the role of each mutated site in the proposed allosteric network. The experimental and simulated data provide insight into key functional residues involved in gating and lipid allostery of K^+ channels. Our findings also have direct implications on the physiology of hKir channels due to conservation of many of the residues identified in this work from KirBac1.1.

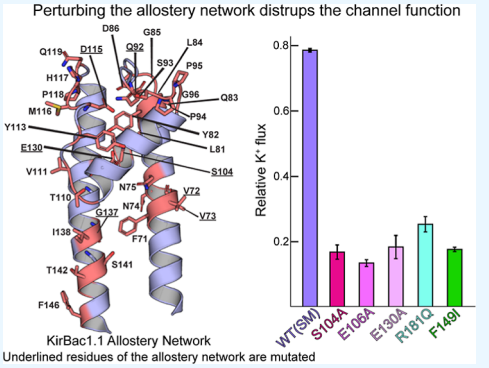

INTRODUCTION

Inward-rectifier K^+ (Kir) channels are integral membrane proteins with important physiological roles in mammalian excitable cells, notably the heart, brain, kidney, and pancreas.[1−4] Although these channels can pass potassium ions (K^+) in both the directions of the membrane, they have a higher tendency to conduct potassium into the cell.[5−8] Thus, these channels drive and establish a charge gradient necessary for crucial processes such as restoring resting potentials in the cardiac tissue, insulin secretion, and muscle contraction.[5,9] There are a number of human diseases that are associated with dysfunction and mutation of Kir channels.[10] These include, but are not limited to, Bartter syndrome which affects kidney, CNS, and vascular function in Kir1.1,[10] Andersen−Tawil syndrome that causes cardiac arrhythmias and skeletal abnormalities, neurocognitive disorders including Parkinson's and short/long QT syndrome in Kir2.X,[11] epilepsy, addiction, alcohol abuse, and familial hyperaldosteronism in Kir3.X,[12] transient neonatal diabetes or hyperinsulinism in Kir6.X,[13] and snowflake vitreoretinal degeneration in Kir7.X.[14] Thus, a better understanding of the channel pathophysiology and disease state mutations could be monitored by the dynamics of key residues in the allosteric network involved in Kir channel gating.

Dependence of Kir channel function on the lipid environment is well documented.[1−4,15−18] Yet, site-specific details of these interactions have not been depicted. There have been many different studies targeting lipid interaction with Kir channels. For example, most mammalian Kir channels require phosphatidyl-4,5-bisphosphate as a primary lipid for activation.[16−18] Cholesterol, another important eukaryotic lipid, plays a vital role in the regulation of Kir channel function.[19,20] Anionic lipids including phosphatidylglycerol (PG), phosphatidylserine, and cardiolipin are known Kir channel effectors, which possess primary and secondary phospholipid-binding sites that are identified in many different channels.[21,22] These protein−lipid interactions include the recruitment of anionic lipids within the inner membrane leaflet and a complex

Received: July 14, 2022
Accepted: November 10, 2022
Published: November 23, 2022

network of interactions behind the selectivity filter (SF) that stabilizes the characteristic "bow-string" conformation.[23] Proper positioning of the channel in the phospholipid bilayer to minimize basal activity and conformational changes associated with the channel's open state are also associated with this phenomenon.[23] Mechanistic studies identified critical residues involved in gating of other K^+ channels sharing homology across subclasses.[21] For example, in K^+ channel streptomyces A (KcsA), the most extensively studied potassium channel, most of these essential residues have been identified.[24−27] This serves as a useful model for mutations of other potassium channels that may share homologous features with KcsA, like those of the Kir family.

In our previous studies, we identified three discrete conformations of KirBac1.1 in inactivating 1-palmitoyl-2-oleoyl-*sn*-glycero-3-phosphocholine (POPC) environment and activating lipid bilayers including 1-palmitoyl-2-oleoyl-*sn*-glycero-3-phospho-(1′-rac-glycerol) (POPG) in a POPC/POPG environment *via* solid-state nuclear magnetic resonance (SSNMR).[23,28] In this state, we observed two different conformations of specific residues within the transmembrane region of the channel that are distinct from those associated with the closed, inactive state in a zwitterionic bilayer.[23] This was the first reported instance of coexisting conformers of a Kir channel. We also identified the three primary lipid-binding arginines that, with mutation of these sites to glutamine (Q), produced an inactive channel regardless of the lipid environment.[28] KirBac1.1 is highly homologous to human Kir (hKir) channels and is thus an excellent model system to explore lipid regulation mechanisms.[29−31] In this work, we present mutants of KirBac1.1 which target and perturb secondary anionic lipid-binding residues proximal to the primary binding site and the mechanisms of activation described above. These mutants were developed using an informed approach based on established homologous mutations, molecular dynamics (MD) simulations, and our previous SSNMR studies.

Below, we employ a fluorescence quenching functional assay[32] to investigate how the proposed mutants affect the K^+ conductance of KirBac1.1.[23] Mutation of a residue in the bow-string motif, D115, was assessed to not affect the activity of the channel when mutated to alanine. However, mutation of the bow string residue E106 in the pore helix, neighboring S104, and E130 in transmembrane helix 2 (TM2) dramatically decreased the K^+ conductance. A series of inactivating valine mutants were also investigated, V72/73/133A. The VV pair V72/73 has been shown to undergo conformational changes associated with anionic lipid activation.[23] An additional inactivating R181Q mutant was observed, which is hypothesized to further disturb the anionic lipid binding leading to channel activation. We investigate mutants of G137, L140, and F149 in TM2 that are involved in the main channel activation allosteric network. These functional data are paired with coarse grain molecular dynamics (CGMD) simulations in an activating, PG-rich environment using the Martini Forcefield.[33,34] MD experiments have been used to good effect to characterize large macromolecular complexes such as protein−protein interactions,[35−40] protein−lipid interactions,[19,20,41] and conformational dynamics of biomolecules.[42−46] These *in silico* experiments contextualize the effect of mutation on how PG interacts with KirBac1.1 *via* PyLipID analysis.[47] It was found that loss of PG residency time on gating arginine residues as a function of mutation *in silico* was correlated with flux *in vitro*. Intrigued, we performed CONtact ANalysis (CONAN)[48] to understand the dynamic effects of mutation on channel dynamics. From our simulations, we observed residue−residue contacts consistent with slide helix, TM, and pore helix motion correlated with dynamics of SF and pore-lining residues. These observations were found to be correlated with both PG residency in simulation and the extent of channel flux *in vitro*. Last, we present some evidence implicating mutational impact on ordering of the bilayer around KirBac1.1, which was previously documented to occur in part as a function of protein−lipid interaction.[28] In aggregate, our results provide insight into functional residues critical for stabilization and allosteric regulation of KirBac1.1, with implications in physiology of hKir channels.

MATERIALS AND METHODS

Molecular Biology. Mutants were generated via site-directed mutagenesis polymerase chain reaction on the KirBac1.1 I131C stability mutant (SM) construct,[49] as described previously.[28] Mutated codon(s) were flanked by tails with a T_m of ∼60 °C (±2 °C) counting each GC pair as 4 °C and each AT pair as 2 °C. The annealing temperature of 60 °C was used and adjusted accordingly based on the presence or absence of DNA bands on agarose gel electrophoresis. Successful reactions were then digested with Dpn1 (1 μL per 50 μL reaction) for at least 4 h at 37 °C before transformation into DH5α *E. coli*. Isolated colonies were chosen to inoculate a 5−10 mL Luria Broth culture, grown overnight, and were then purified using the Macherey−Nagel miniprep kit. All purified plasmids were confirmed *via* sequencing.

Expression and Purification. The expression and purification of KirBac1.1 (I131C) were performed as described previously.[50] In summary, a 0.5 L of Terrific Broth + PO_4 culture media was used for the growth, and cultures were induced at an OD_{600} of approximately 1 with 1 mM isopropyl β-D-1-thiogalactopyranoside. Cells were harvested after ∼18 h of expression and stored at −80 °C until needed. Frozen cells were resuspended with lysis buffer (50 mM Tris-Base pH 8, 150 mM KCl, 250 mM Sucrose, and 10 mM $MgSO_4$) and lysis cocktail [1 mM benzamidine, 1 mM phenylmethylsulfonyl fluoride, 0.2 mg/mL lysozyme, 0.2 mg/mL RNAse, and protease inhibitor tablets] at 5 mL/g cells. After homogenization, 30 mM decyl-β-D-maltopyranoside was used for extraction (between 3 and 4 h). Debris was removed *via* ultracentrifugation, and the supernatant was filtered. Samples were loaded into a 5 mL HisTrap column (Cytiva) pre-equilibrated with wash buffer [50 mM Tris-base pH 8, 150 mM KCl, 10 mM imidazole, 2.5 mM *n*-dodecyl-β-D-maltoside (DDM)] and eluted with elution buffer (50 mM Tris-Base pH 8, 150 mM KCl, 250 mM imidazole, 2.5 mM DDM). The eluted protein was loaded onto a desalting column and immediately exchanged into a low imidazole exchange buffer (50 mM Tris-Base pH 8, 150 mM KCl, 1 mM EDTA, 5 mM DDM). The desalted protein was diluted to around 50 mL with exchange buffer (less than 1 mg/mL) for overnight storage at 4 °C. The next day, the diluted protein was concentrated with a 100 KDa ultrafiltration disc and an appropriately sized Amicon stir cell concentrator to be loaded on a size exclusion chromatography column equilibrated with exchange buffer. The tetrameric fraction was collected for downstream processes.

Sample Reconstitution. A lipid mixture of 3:2 (w/w) POPC/POPG dissolved in $CHCl_3$ was dried under N_2 gas and put under vacuum overnight. Dried films were then solvated at

https://doi.org/10.1021/acsomega.2c04456
ACS Omega 2022, 7, 43621−43634

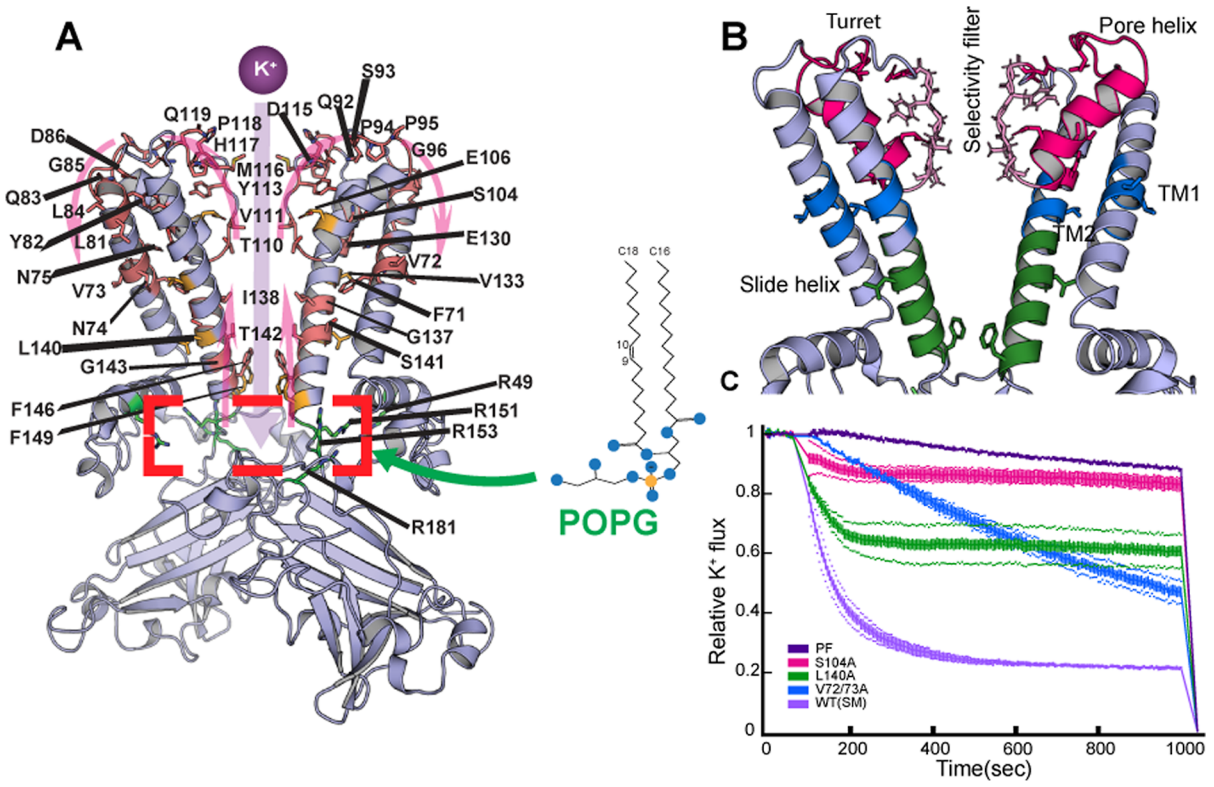

Figure 1. (A) Proposed allostery network of KirBac1.1 triggered by the action of POPG (dark pink)23 in gating the channel. The originally proposed directionality of the allosteric network trigged by opening the HBC is depicted by purple arrows. The residues previously found to have marked structural changes (mapped as resolvable changes in chemical shift) between the open and closed states of the channel are depicted in pink. Residues targeted in this study not previously identified *via* SSNMR are depicted in orange. Key lipid-tethering arginine residues are in green. The PG lipid headgroup lipid-binding pocket is marked with a red dashed box. (B) Anatomy of the transmembrane region of KirBac1.1 (7SWJ). SF residues (TVGYG) are highlighted as light pink; pore helices, turret, and bow string mutants are colored hot pink; transmembrane valine mutant regions are colored blue; mutants in the TM2 region are colored green. (C) K^+ flux assay for KirBac1.1 WT stability mutant (SM) reconstituted in an activating 60:40 POPC/POPG lipid environment. Representative traces for several mutants are included. Fluorescent traces for all mutants are available in the Supporting Information (Figure S1). Loss in fluorescent signal corresponds to K^+ flux, confirming channel activity.

5 mg/mL in K^+ Buffer (20 mM K-HEPES, 150 mM KCl, 1 mM EDTA, pH 7.4 w/HCl) for the K^+ flux assay or Na^+ Buffer (20 mM Na-HEPES, 150 mM KCl, 1 mM EDTA, pH 7.4 w/HCl) for the Na^+ flux assay, plus 18.5 mM 3-[(3-cholamidopropyl)-dimethylammonio]-1-propane sulfonate] *via* brief sonication. The sized protein was concentrated to 0.5−1 mg/mL using a 100 KDa ultrafiltration disc and an appropriately sized Amicon stir cell concentrator. Purified and concentrated KirBac1.1 was then added to a ratio of 3:200 protein/lipid (w/w) and annealed for 30−60 min before the first 30−40 mg addition of Bio-Bead SM-2 Resin (Bio-Rad) for detergent removal. Subsequent additions of Bio-Beads were performed every 12 h until samples appeared cloudy, and no membrane leakiness was observed when collecting baseline fluorescence.

Potassium and Sodium Efflux Assays. K^+ flux assays were performed and analyzed as described previously.[23] In summary, proteoliposomes were incubated with 100 μM 9-amino-6-chloro-2-methoxyacridine dye for 15 min at room temperature and then diluted 1:20 using Na^+ buffer (20 mM Na-HEPES, 150 mM NaCl, 1 mM EDTA, pH 7.4 w/HCl) in a 96-well plate. An additional 1:1 dilution with Na^+ buffer was performed on transferring to the 384-well plate. A baseline, with excitation and emission wavelengths of 410 and 480 nm, was read for 1 min, and then 10 μL of 80 μM (5×) carbonyl cyanide *m*-chlorophenyl hydrazone (CCCP) was added to initiate the K^+ flux. Data were collected for 15 min. Finally, 1 μL of 10 nM valinomycin was added and read for 1 min to determine the maximum K^+ flux. Na^+ flux assays were performed identically to the K^+ flux assay as described above but with a few substitutions. The inner liposomal K^+ buffer was replaced with the Na^+ Buffer as described during reconstitution, while the outer liposomal Na^+ Buffer was replaced with a Li^+ Buffer (20 mM HEPES-free acid, 150 mM LiCl, 1 mM EDTA, pH 7.4 w/KOH) used for making the initial 1:20 and last 1:1 dilution. Valinomycin was exchanged for the Na^+ ionophore, monensin, and added at the end of the assay to measure the maximum Na^+ flux. All flux data were normalized using the following equation

$$F_N = (F - F_V)/(F_B - F_I)$$

where F_N is the normalized fluorescence, F is the measured fluorescence, F_I is the minimal fluorescence from the ionophore (valinomycin for the K^+ assay and monensin for the Na^+ assay) addition, and F_B is the baseline fluorescence.

The relative flux of K^+ or Na^+ was determined using the following equation

$$(F_b - F_a)/F_b$$

where F_b is the fluorescence before adding CCCP and F_a is the fluorescence before adding valinomycin or monensin.

https://doi.org/10.1021/acsomega.2c04456
ACS Omega 2022, 7, 43621−43634

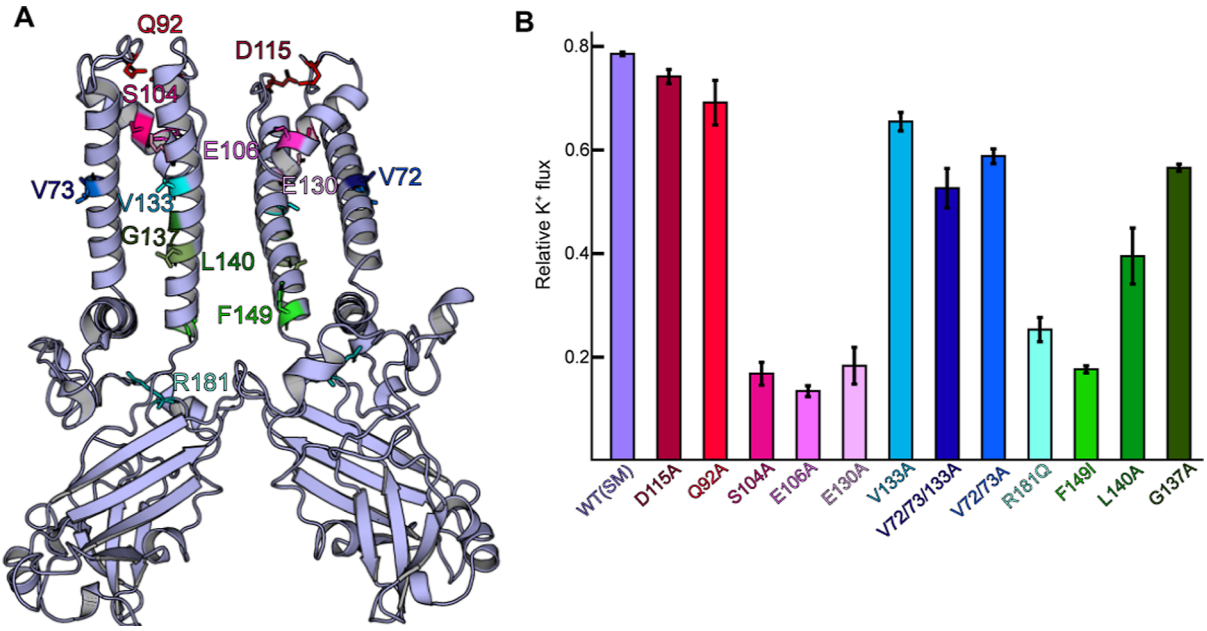

Figure 2. Presentation of assay results. (A) Mutations mapped onto the structure of KirBac1.1 (PDB ID: 7SWJ) color coded by type. Red-shaded mutations are located in the SF region, blue-shaded mutations impact lipid interaction, and green-shaded mutations influence the allosteric network linking PG interaction and channel activation. (B) K^+ flux assay results for each mutant color coded as in (A). Data are presented as relative K^+ flux normalized to total flux carried out by the K^+ ionophore valinomycin. Data are extracted from fluorescent traces in Figure S1.

MD and PyLipID Analysis. The KirBac1.1 structure PDB 7SWJ was used for MD analysis.[51] Mutants were generated using the Pymol mutagenesis wizard. All structural inputs were oriented using the PPM 2.0 webserver[52] (https://opm.phar.umich.edu/ppm_server2). CGMD input files were generated using the CHARMM-GUI[53,54] Martini Maker[55,56] (https://charmm-gui.org/?doc=input/martini.bilayer). System parameters included a 50 nm thick water layer, a box size of 150 nm, and 50 mM NaCl at a temperature of 273.15 K. Martini parameterizations of K^+ and Na^+ were identical. MD was performed in GROMACS version 2020 using the Martini2.2 forcefield.[33,57,58] Minimization and equilibration molecular dynamics parameter (MDP) files were the default CHARMM-GUI outputs. Production made use of a custom MDP file first described by Duncan *et al*[20] and more recently by Borcik *et al*.[19] Minimization and equilibration were performed with the Berendsen barostat,[59] v-rescale thermostat, and reaction-field electrostatics. Production MD was performed as in minimization and equilibration but with the Berendsen thermostat. The gmx order tool was used to calculate the average acyl bead order parameters throughout simulation. PyLipID was used to quantify the lipid−protein interaction throughout production MD using standard start and end cutoffs of 0.55 and 1.0 nm, respectively.[47] CONAN (https://github.com/HITS-MBM/conan) was used to map inter-residue contacts throughout coarse grain trajectories.[48] Gridmat-MD (https://github.com/jalemkul/gridmat-md) was used to generate average bilayer thickness values, calculated as the distance between PO_4 beads of the inner and outer leaflets, and using a grid size of 30 × 30.[60] All simulations and analysis were performed on the Texas Tech High Performance Computing Center and NMRbox.[61]

Sequence Alignment Analysis. The alignment was performed using the following protein sequences, including accession numbers from Uniprot: O60928 (hKir7.1), P48048 (hKir1.1), P78508 (hKir4.1), Q9NPI9 (hKir5.1), Q14654 (hKir6.2), Q14500 (hKir2.2), P63252 (hKir2.1), P48549 (hKir3.1/GIRK1), P48051 (hKir3.2/GIRK2), P83698 (KirBac1.1), D9N164 (KirBac3.1), and P0A334 (KcsA). Amino acid sequences were aligned with the Clustal Omega Alignment tool[62] and visualized with ESPript3.0.[63]7SWJ was used for the homology heat map of the proteins aligned where the conservation score was determined as follows: 1 point for the same residue, 0.5 points for the same residue group type, and 0.25 points if the residues were either the same length, charge, or aromaticity, for a maximum total of 11 points.

RESULTS

KirBac1.1 WT. In our previous study we used SSNMR and functional assays to determine the structural details of KirBac1.1 in the closed state (POPC lipid environment) and open state (POPC/POPG lipid environment).[23] We observed two different conformers of the protein in the POPC/POPG lipid environment, distinct from the inactive conformer in the POPC lipid environment. These residues were mostly located in the transmembrane region of the protein which led us to propose an allostery network in KirBac1.1 which is triggered by activating lipids (Figure 1A). This network encapsulated the PG binding pocket comprised of R49, R151, and R153, TM residues lining the pore such as I138 and T142, the canonical TVGYG SF motif, and hydrogen bonding network residues in the pore helix and turret that provide support for the SF (Figure 1A). Though we have based this hypothesis on the observed chemical shift perturbations in inactive and activating lipid environments, it should be noted that many details of the proposed network remain opaque. While we proposed a directionality to this network (purple arrows Figure 1A), the temporal ordering of these allosteric remodeling events is unknown. We hypothesize that the structural rearrangements are the result of interaction between anionic lipids (PG) and arginine residues in the activation gate leading to a "domino

https://doi.org/10.1021/acsomega.2c04456
ACS Omega 2022, 7, 43621−43634

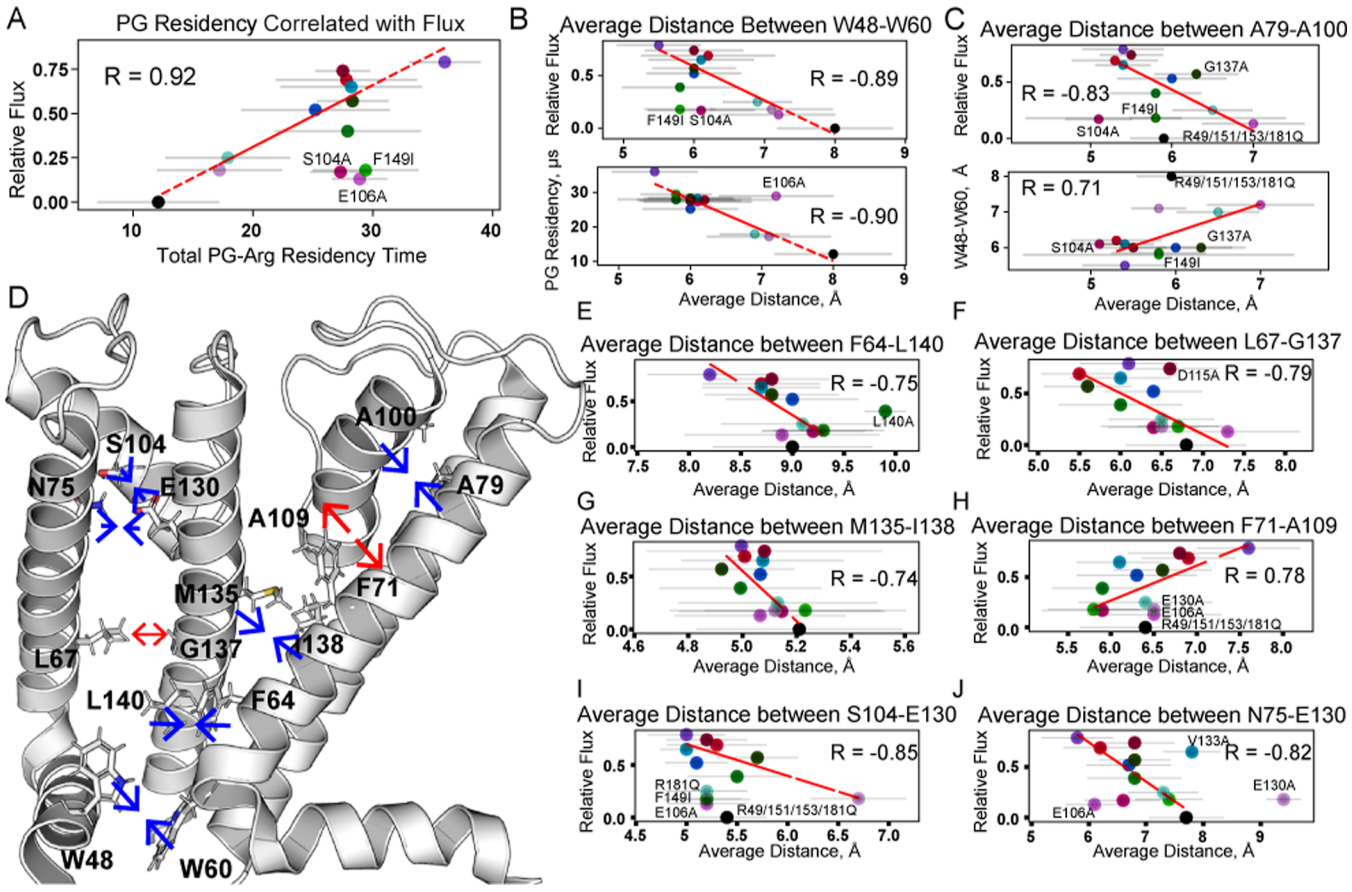

Figure 3. Correlation analysis of KirBac1.1 WT (SM) compared to mutations from CGMD using PyLipID and CONAN. (A) Correlation between % flux and PG residency time on gating arginines calculated with PyLipID. CONAN was used to calculate the average distance ± RMSF throughout simulation and across replicates for (B) W48-W60 and (C) A79-A100, plotted onto the TM region of KirBac1.1 (D), where blue arrows denote interaction residues that get closer, while red arrows indicated residues that grow apart as flux and PG residency time increase. Only adjacent subunits are shown for clarity. Correlation analysis is further presented for contact between (E) F64-L140, (F) L67-G137, (G) M135-I138, (H) F71-A109, (I) S104-E130, and (J) N75-E130. In all cases, relationships are noted between these contacts, PG residency, and functional activity *in vitro*. Labeled residues on each plot denote outliers not included in the correlation analysis.

effect" involving both transmembrane helices, the pore helix, the turret, and the SF (Figure 1A,B).[23]

In this work, we use KirBac1.1 to investigate the functional properties of Kir channels after mutation of residues hypothesized to be involved in gating, hydrogen bonding, and protein−lipid allosteric interactions. The plasmid in this study contains the SM I131C, reported to have no effect on the activity compared to true wild type (WT),[49] though a subsequent study showed that some mutations at this site can radically change channel properties.[64] The I131C mutations stabilize the tetramer during heterologous production and purification. Fluorescent K^+ and Na^+ flux assays were used to determine the functionality of the mutants in the standard activating environment (POPC/POPG, 60:40 percent by mass).[32]Figure 1A shows the proposed allosteric network in Kirbac1.1 in the presence of the activating lipid (POPG). Figure 1B shows the anatomy of the KirBac1.1 structure (PDB 7SWJ), highlighting key regions.[51]Figure 1C shows the K^+ flux assay trace of the WT (SM), confirming the channels' activity, as well as representative fluorescent flux traces for each group of mutants. All traces are available in the Supporting Information (Figure S1). Na^+ flux assays were also performed for select mutants to determine the effect of the mutation on the selectivity of the channel (Figure S2).

Interactions Proximal to the SF. As mentioned above, our SSNMR data revealed multiple residues involved in conformational changes at the extracellular end of the transmembrane region near the SF. These observations informed our decisions on mutations in this region.[23] Two of these residues comprise the bow string motif, which is formed by an aspartate in the selectivity loop (D115) and a glutamate in the pore helix (E106). The hydrogen bonds between these D and E residues and multiple interactions between other side chains in this region stabilize the SF and are also crucial to the channel function.[65] Mutations of residues in this region are presented in shades of red (Figure 2). Alanine mutations to the residues near the top of this region, including Q92 and D115, did not significantly impede the channel function. However, alanine mutants of residues in the pore helix or packed against the pore helix, including S104, E106, and E130, were nearly inactive (Figure 2B). Two of these residues, S104 in the pore helix and E130 in TM2, may form a crucial contact with N75. Previous work reported that E106A was activating in true WT KirBac1.1,[64] and thus we speculate the observed loss of activity here is due to synergistic effects between E106A and the stability mutation I131C. E130 likely forms additional interactions that the alanine substitution disrupts. This interaction is intra-subunit and ties TM2 to the pore helix.

https://doi.org/10.1021/acsomega.2c04456
ACS Omega 2022, 7, 43621−43634

Perturbation of Lipid-Binding: Transmembrane Valines and Gating Arginines. One of the sites of long-distance conformational exchange that was identified via SSNMR was the V72/73 pair.[23] These residues are proximal to other identified regions of the allosteric network. However, they are also poised to directly interact with lipid acyl chains. We hypothesized that this valine pair plays a support role for a well-known characteristic kink that is located in TM2 at G137. Thus, the motion of TM2 requires a support and control mechanism to correctly mediate motion during conformational exchange. Loss of these residues is hypothesized to destabilize the kink region and thus reduce channel activity, which is observed (Figure 2, blue shades). V to A mutations, in this case, should not significantly disrupt a helical hinge motion around G137 but limits possible steric clashes with the lipid acyl chain. V133 is also positioned to form similar interactions and is located proximal to the TM2 hinge. In aggregate, this analysis provides plausible reasoning for why V133A, V72/73A, and V72/73/133A mutations were partially but not fully inactivating.

Significant results discussed in previous work involved disruption of the phospholipid head group binding pocket by mutation of gating arginines (R49/151/153) to glutamine. The result of these mutations was a loss of channel activity. Here, we also determine the role of R181Q in channel activation *via* K^+ flux assays. Figure 2 (cyan) indicates that K^+ flux has decreased dramatically, suggesting an addition to the family of KirBac1.1 gating arginine residues.

Perturbating Allosteric Regulation: G137A, L140A, and F149I. Residues G137, L140, and F149 are located on TM2 (Figure 2A, green shades). In all cases, mutation of these residues negatively impacts channel activity (Figure 2B, green shades). G137 is believed to be a hinge to allow free range of conformational change.[23] Mutation of this residue may simply hamper requiring gating motions. We proposed, based on chemical shift perturbations, that the side chain of L140 may form a crucial contact along the allosteric pathway, thus explaining the mutant's loss of function. In the tetramer of KirBac1.1, four F149 residues come together at what is described as the helical bundle crossing (HBC). These residues may undergo a "swinging out" motion during the channel's conformation change. Thus, they are expected to have strong interplay with proper gating and allosteric regulation of the channel. When mutated to isoleucine, dramatic loss of total conductance is observed. This may result from the loss of a pi-stacking interaction.

CGMD: Effects of Mutation on PG Interaction and Channel Dynamics. All mutations presented were selected due to hypothesized impact on protein function either through perturbation of protein structure or direct interference with the lipid tethering activation mechanism. To gain insight into how respective mutations change the dynamic structure and lipid interaction with each mutant channel, CGMD and subsequent trajectory analysis were performed. Starting structure files for the SM and all subsequent mutants were built into CGMD systems consisting of 3:2 PC/PG using CHARMM-GUI.[53,54] Production MD was carried out for 10 μs for each of five replicates per structure input for a total of 650 μs of simulation time. PyLipID[47] was then used to calculate PG interaction with the WT (SM) and each mutant throughout the simulation (Figure S3). At no point during the simulations was the HBC fully open; thus the following analysis is limited to the start of the activation process. Compared to the SM residency time, PG interaction is significantly impacted. Indeed, when total PG residency time throughout the simulations is plotted against % relative flux, a general trend is observed where flux *in vitro* is well correlated with the PG residency time on gating arginines *in silico* (Figure 3A, R = 0.92). R49, R151, and R153 were previously shown to be the binding loci for PG-driven activation of KirBac1.1,[28] while R181 was included due to observations novel to this work. Of these arginine residues, R181 is the most buried structurally and has the most varied residency time *in silico*. It is also observed to be much less active than expected if R181 were simply another gating arginine. Thus, there may be an additional activatory role for this arginine to be investigated in a future work. Considering R49/151/153/181Q, it is no surprise this mutant would experience the least PG interaction. However, many other mutations are not located in the lipid-interacting regions; thus it was an intriguing observation that their mutation impacted PG interaction with these residues. Outliers from this analysis include S104A, E106A, and F149I. S104 and E106 are likely linked to SF stability during K^+ conductance, and F149 may directly stabilize the open HBC. Omitting these, the correlation coefficient becomes 0.92, showing good agreement between interaction with gating arginine residues and K^+ flux as a function of mutation *in vitro*. However, this result is surprising. Previously we hypothesized that anionic lipids triggered allostery starting from the HBC and that disruption of this network would reduce K^+ flux. However, these results suggest that allostery may also govern the ability of gating R residues to substantively interact with POPG.

We next performed CONAN calculations to pinpoint how mutation impacts the dynamic structure of the channel *in silico*.[48] We first observed that PG residency in simulation increases as W60 in one subunit gets closer to W48 in the next (R = −0.90), which is in turn correlated with flux *in vitro* (R = −0.89, Figures 3B and S4A). We attribute this contact to "sliding" of the slide helix, speculated to be an important event during channel activation. Outliers of this observation are, unsurprisingly, S104A, E106A, and F149I, indicating mechanisms of functional perturbation unrelated to interference with channel activation as described above. In general, this motion is accompanied by an outward motion of the pore helix toward TM1 (R = 0.71, Figures 3C and S4B), measured by the average distance between A79 in TM1 and A100. This observable is also correlated with flux *in vitro* (R = −0.83), though less well conserved than other correlations and is independent of PG residency time (R = −0.22). These interactions are presented on adjacent subunits of KirBac1.1 for visualization purposes (Figure 3D).

We were curious what changes in contacts might occur within the transmembrane region that could lead to modulation of pore helix behavior. We found that the L140-F64 intra-subunit distance (Figure 3E, R = −0.75) and the L67-G137 inter-subunit distance (Figure 3F, R = −0.79) both decrease with increased flux, PG residency, and a decreased W48−W60 distance (Figure S4C,D). Of the former, L140A is a clear outlier which is likely related to loss of function in the mutant. Conversely, G137A falls squarely within the observed trend of the latter. *In vitro* G137A may be less able to kink, leading to less overall activation due to perturbation of the activation mechanism we cannot observe in our simulations. Furthermore, the I138 and M135 intra-subunit distance is negatively correlated with flux (Figure 3G, R = −0.74) with no outliers. A similar trend is observed for PG residency (R =

https://doi.org/10.1021/acsomega.2c04456
ACS Omega 2022, 7, 43621−43634

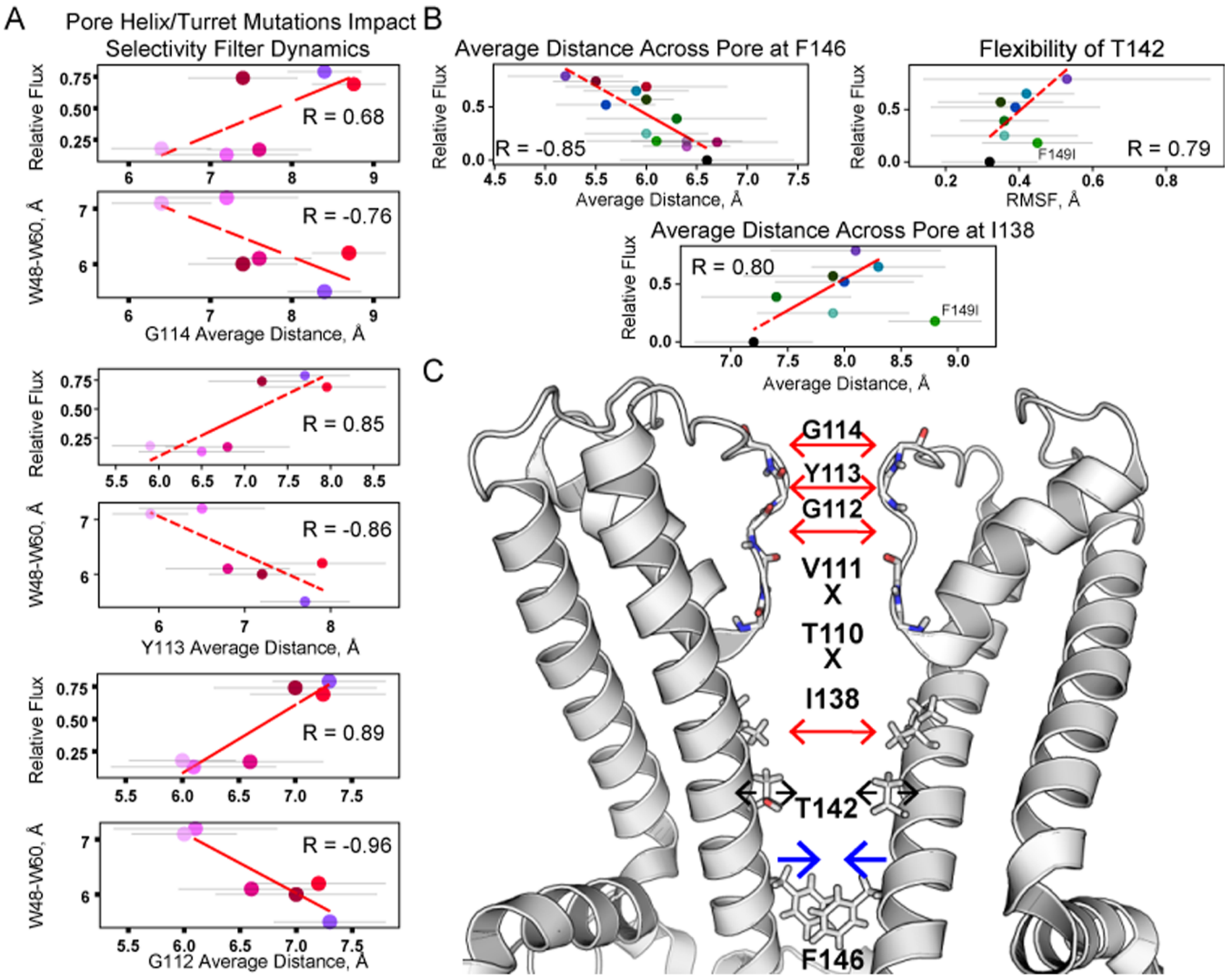

Figure 4. Correlation analysis of KirBac1.1 WT (SM) compared to mutations from CGMD using CONAN. Data are presented as the average distance ± RMSF throughout simulation and across replicates for (A) SF residues including G112, Y113, and G114 and (B) pore-lining residues I138, T142, and F146. In all cases, relationships are noted between these contacts, PG residency, and functional activity *in vitro*. Labeled residues on each plot denote outliers not included in the correlation analysis. (C) Summarization of contacts presented in (A,B) mapped onto the structure of KirBac1.1 (7SWJ). Opposing subunits are shown for clarity. The directionality of contacts denotes those that were more likely to occur as a function of PG residency time in silico and relative flux *in vitro*. Blue arrows denote interaction residues that get closer, while red arrows indicate residues that grow apart as flux and PG residency time increase.

−0.73) and the W48−W60 distance (R = 0.71) though F149I is an outlier in both cases (Figure S4E). In addition, the F71-A109 intra-subunit distance is positively correlated with flux (Figure 3H, R = 0.78). This observation is loosely correlated with PG residency (R = 0.63) and not at all (R = −0.08) to the W48−W60 distance (Figure S4F). Overall, it does appear that the base of TM1 increases the general contact with the slide helix and TM2 of the adjacent subunit, owing to these observations coupled with the W48−W60 contacts described above. This is translated up the helices, bringing M135 and I138 of adjacent subunit closer together. A109 was observed to have an enormous chemical shift perturbation during activation in our previous work, and thus pitching of the very base of the pore helix away from F71 may be related to the activation pathway. At the same time, it is observed that the rest of the pore helix tilts *toward* TM1 and TM2. In addition to A79-A100 contact, tighter interaction between S104-E130 (R = −0.85) and N75-E130 (R = −0.82) is observed to be correlated with flux (Figures 3I,J, S4G,H). E106A and E130A are outliers of both this trend and that observed for F71-A109, suggesting that these mutants facilitate untethering of pore helix support as originally hypothesized.

We next characterized SF dynamics as all pore helix/turret mutants were designed to perturb the SF support network (Figure S5). Here, data are presented as the average distance between each residue and its neighbors in adjacent subunits. Indeed, a strong correlation was observed between these mutants and "pinching" of the SF for G112, Y113, and G114 in the canonical TVGYG sequence (Figure 4A). For example, inter-subunit distance between Y113 residues increases with flux (R = 0.85) and PG residency time (R = 0.73) and is negatively correlated with W48−W60 distance (R = −0.86). Similar trends are observed for Y113 and G114 but not T110 and V111 (Figure S5). Considering TM and HBC mutants, there is a measurable effect of these mutants on the dynamics of pore-lining residues that are, in general, well correlated with

https://doi.org/10.1021/acsomega.2c04456
ACS Omega 2022, 7, 43621−43634

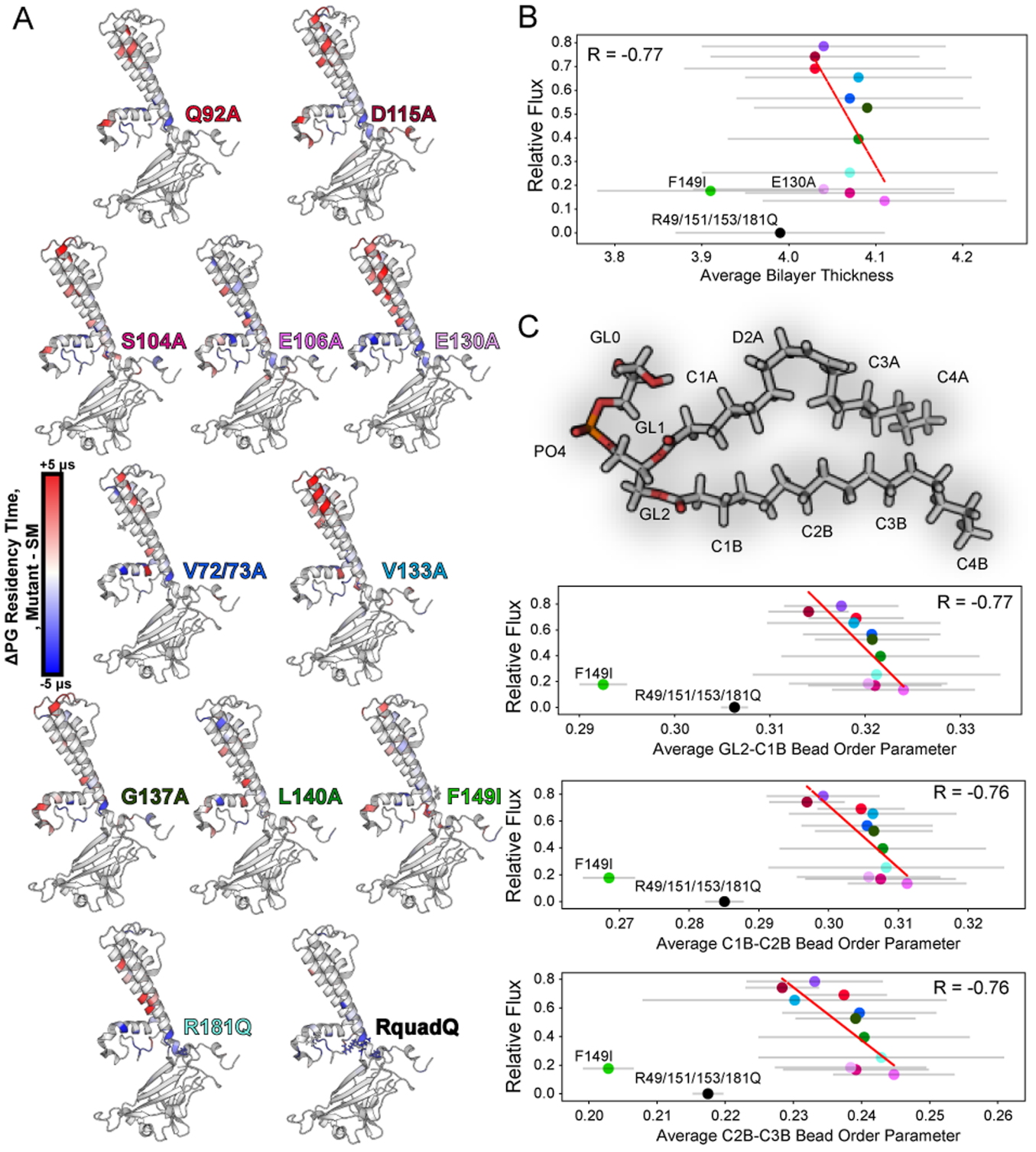

Figure 5. Effects of mutation on the global PG residency time and bilayer properties. (A) Change in POPG residency time upon introduction of indicated mutations. SM residency time for a given residue is subtracted from the residency time of that residue in the mutant simulations. Red color indicates greater mutant residency time, while blue indicates less residency time compared to SM. Great change in PG residency time is observed in most cases, indicating a perturbing effect of mutation on the activation mechanism. (B) Correlation between % flux and average bilayer thickness from CG simulations. A loose negative correlation between the two parameters is observed. (C) Correlation between % flux and average palmitoyl acyl bead order parameter throughout CG simulations. Acyl bead martini parameterization (black) is mapped onto the atomistic structure of POPG. A loose negative correlation between acyl ordering and function is observed. Data are presented as mean ± std. Color coding of points in (B,C) corresponds to labels in (A). Labeled residues in (B,C) indicate uncorrelated outliers excluded from linear fits.

flux, PG residency, and distance between W48 and W60 on adjacent subunits (Figures 4B and S6A−C). These residues include I138, T142, and F146 at the HBC, all of which were previously identified to have significant chemical shift perturbation when transitioning between the inactive and active channel conformations.[23] Perhaps most interesting is

https://doi.org/10.1021/acsomega.2c04456
ACS Omega 2022, 7, 43621−43634

consideration of the distance across the pore at F146. Here, distance decreases as flux increases for *all* residues ($R = -0.85$) with no outliers. This observation is also well correlated with PG residency ($R = -0.74$) with S104A and E106A again as outliers and contact between W48 and W60 ($R = 0.84$) with S104A and L140A as outliers. Considering only TM/HBC mutants, the average distance between I138 residues across the pore also increases as flux increases ($R = 0.80$). At the same time, T142 becomes more flexible ($R = 0.79$) measured *via* RMSF throughout the simulation. I138 distances and T142 flexibility are also negatively correlated ($R = -0.79$ and -0.88, respectively). Thus, for TM/HBC mutants' function and PG residency increase as the pore at I138 expands, F146 constricts, T142 conformational fluctuation increases, and W48−W60 distance decreases.

Our results from CONAN analysis paint an interesting picture, as summarized in Figure 3F. In the WT channel, our data suggest that PG interaction with gating arginine residues drives slide helix motion which is coupled to outward motion of the pore helix, opening of the SF filter, and modulation of pore-lining residue dynamics that could be related to K^+ flux *in vitro*. Mutation to key regions of the protein impacts these events, driving reproducible pinching of the SF, negative modulation of pore residue dynamics, and loss of PG interaction with the gating arginine residue that could ultimately culminate in the loss of function *in vitro*. S104A, E106A, and F149I appear consistently as outliers of these observations. In the case of S104A and E106A, their *in vitro* flux activity is far lower than expected from contact scores and PG residency time. We conclude that these mutations may be more likely to induce full SF collapse that will not be observable in coarse grain simulations. F149, on the other hand, is found within the hydrophobic pocket surrounding the pore[66] and thus may affect coupling of PG binding to pore opening. Indeed, F149I is *not* an outlier when contact between F149 and W60 is correlated with flux ($R = 0.77$), PG residency time ($R = 0.87$), and W48−W60 contact ($R = -0.78$) nor to modulation of distance across the HBC measured *via* F146 (Figure S6A,D).

CGMD: Effects of Mutation on Bilayer Properties. It was curious that pore helix/turret mutations could have an effect on the PG residency and dynamics of the gating residue F146, but we did not conversely observe TM/HBC mutational effects on SF dynamics. When considering plots of change in the residency time as a function of mutation, it is clear that SF support mutations have a fundamental impact on how PG interacts with the channel (Figure 5A). We previously showed through SSNMR experiments that KirBac1.1 orders the bilayer around itself and that this phenomenon is partially abolished when R49, 151, and 153 are mutated to glutamine.[28,50] To investigate if our mutations could induce similar phenomena, we also performed analysis of bilayer properties. Gridmat-MD[60] was first used to assess bilayer thickness of the final frames of each trajectory. While the bilayer thickness is on average very similar (Figure S7), a trend is observed where there is a negative correlation between the average bilayer thickness and KirBac1.1 mutant activity (Figure 5B). This was again surprising given previous observations of bilayer ordering around KirBac1.1 as higher degrees of order are correlated with thicker membranes. This was assumed to in turn be correlated with KirBac1.1 function since the R49/151/153Q mutant attenuated ordering and was functionally inactive.[28] Outliers of this trend include E130A, F149I, and R49/151/153/181Q. Thus, our analysis of the R49/151/153/181Q simulation agrees with previous studies of the Triple Q mutant, which seems to be functionally equivalent to F149I based on similar patterns in the change in PG residency and bilayer thickness. Of the other mutants, it is curious that an increase in the average bilayer thickness is correlated with a loss in function, given this established relationship. A relationship between thicker bilayers and increased ordering is also expected. To establish an explicit correlation, average order parameters for Martini acyl beads throughout simulations were calculated (Figures 5C, S8). A similar trend is observed as for bilayer thickness, establishing that an increase in the bilayer thickness is related to an increase in acyl ordering, which is in turn correlated with decreasing function. Outliers of this trend are again F149I and R49/151/153/181Q, where these mutations attenuate acyl ordering. R49/151/153/181Q abolishes PG lipid binding and was previously shown through the TQ mutant to attenuate ordering, and hence this result is expected. F149I was not, and it is not immediately clear why this is the case but could be related to proximity with the arginine pocket.

Considering that many of these mutations appear to predominantly influence KirBac1.1 interaction with PG in the outer leaflet (Figure 5A), it may be concluded that the increased ordering correlated with the loss of function is leaflet-specific. This would serve to reconcile the seemingly juxtaposed gating bundle PG residency correlation with function and the increased ordering correlated with loss of function. While the range of error bars in Figures 5B,C and S7 dictate that caution should be taken during interpretation of CGMD data, many different analytic methods were performed to reach these conclusions. Though the changes observed are small and in general within error of each other, multiple datasets corroborate the trends observed. In aggregate, our data seem to suggest that there is a so-called "goldilocks condition" for how ordered the bilayer should be to facilitate KirBac1.1 function. It may be that our observations of ordering induced by KirBac1.1 are a byproduct of the activation mechanism rather than a feature and that too much ordering plays a role in decreased function. These observations are highly intriguing and suggest future all-atom MD, and SSNMR characterization of these mutants will be a worthy pursuit.

DISCUSSION

The pore helix and adjacent regions were targeted because of their observed involvement in channel gating. These residues support the SF *via* hydrogen bonding and steric contacts. It is known that the bow string residues D115 and E106, which may be protonated, likely form a crucial hydrogen bond in this region. S104 and Q92 were selected because of the potential hydrogen bonding network interaction with N75 and H124, respectively.[23] Previous results presented by Matamoros and Nichols indicated that E106A was activating rather than inactivating for channel collapse[64] in a manner equivalent to E71 in KcsA.[26] Our results may be fundamentally different due to use of the I131C stability mutant rather than true WT KirBac1.1, which could have some influence on mutant behavior. Regardless, from our assay and MD-derived PG interaction data, we hypothesize that these residues are important for a non-collapsed SF conformation.

TM1 mutations were primarily focused on the valine residues with peculiar SSNMR chemical shifts that revealed multiple conformations of V72 and V73.[23] These residues were

https://doi.org/10.1021/acsomega.2c04456
ACS Omega 2022, 7, 43621−43634

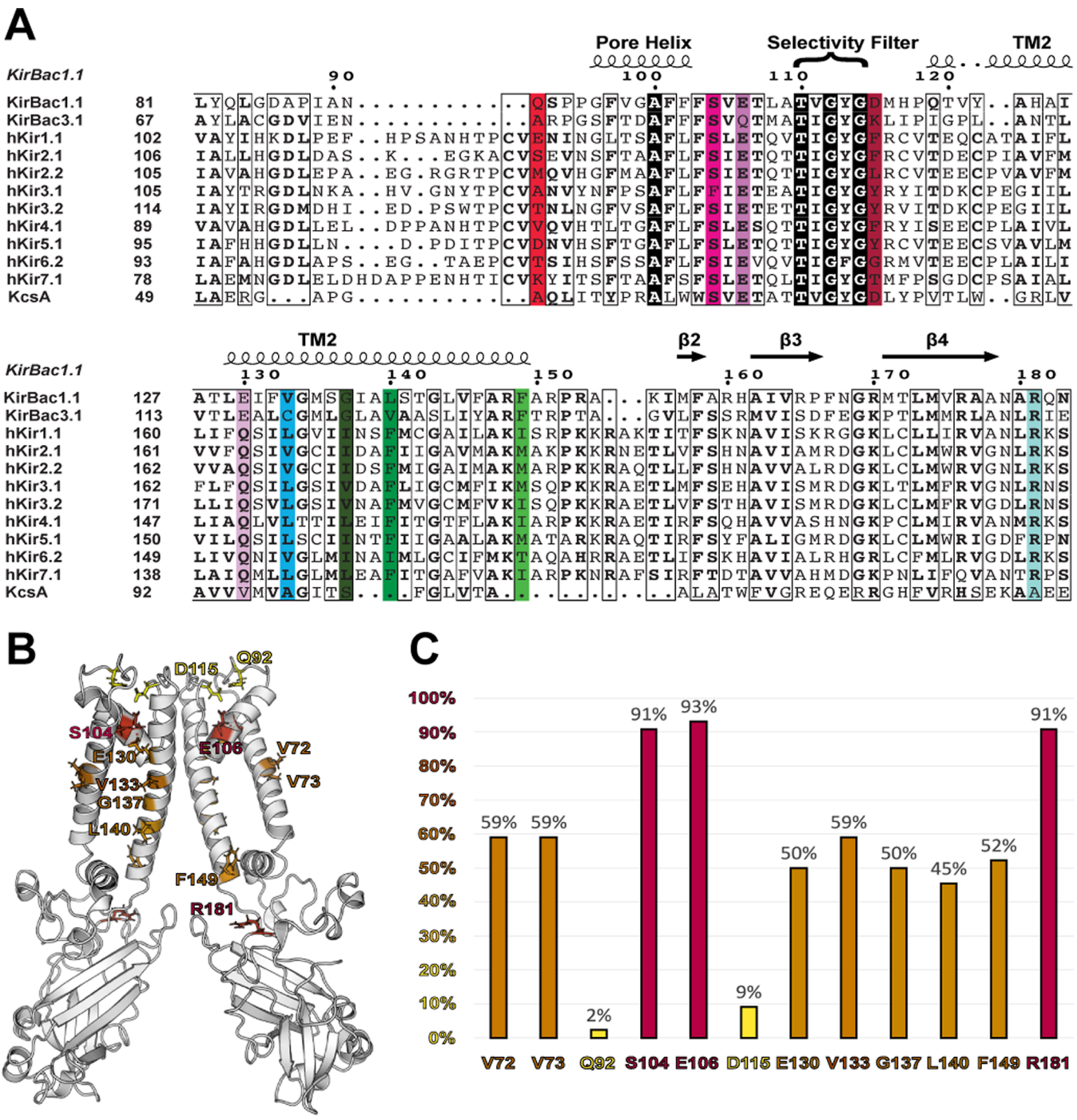

Figure 6. KirBac1.1-K^+ channel homology. (A) Sequence alignment of KirBac1.1, KirBac1.3, human Kir (hKir) channels, and KcsA with secondary structure elements from KirBac1.1 outlining residue position to secondary structure. Mutant positions presented in this paper are color coded as in previous figures above. (B) KirBac1.1 residues investigated in this work presented by degree of conservation in other K^+ channels as a heatmap projected onto the 7SWJ structure. Residues outlined that are highly homologous are depicted in red, and transition as a gradient in color to the least homologous shown in yellow. (C) Bar graph depicting percentage of homology mapped onto (B). Percent (%) homology in (B,C) incorporates degree of similarity based on charge, polarity, aromaticity, and so forth (see Materials and Methods).

postulated to form a concerted pivot point in the channel implying an allosteric effect and/or lipid acyl chain interaction. Such an interaction may grant stability or cause large allosteric effects during conformational change to the active, conductive state. Through lipid-acyl chain and PG residency time throughout CGMD trajectory, we determine that while the valine pairs have little to no interaction with acyl chains, they *do* have a dramatic effect on the arginine-PG residency time. More complex interrogation of this mechanism may prove an interesting avenue for future experimentation.

It was initially suspected that R181 in the flexible linker region may also be associated with binding of the headgroups of anionic lipids, originating from previous work mutating R49, R151, and R153 to glutamine to abolish anionic lipid activation.[23,28] Loss of function of the R181Q mutant in flux assays paired with loss of PG interaction in MD simulations

https://doi.org/10.1021/acsomega.2c04456
ACS Omega 2022, 7, 43621−43634

indicate that R181 has a clear role in lipid activation of KirBac1.1 in addition to R49, 151, and 153. Indeed, PG headgroup interaction with arginine residues in the R181 mutant is quite similar to when all four residues are mutated, albeit to a lesser extent. This is mirrored by R181Q activity compared to the complete loss of activity expected for the R49/151/153/181Q mutant.

Residues along TM2 like the glycine hinge G137, L140, and the gatekeeping F149 at the base of the pore were in part targeted for potential allosteric effects from acyl chain interactions in addition to perturbation of allosteric intra-protein communication. Additionally, F149 was targeted to test if it had major effects on gating mechanisms at the base of the channel to see if the aromaticity was used as a support for proper gating of K^+ ions. Separately, E130 was chosen to test whether the matrix of interactions behind the SF was limited to only the turns and slide helix or if polar (potentially charged) side chains in the TM region play a role. Loss of function in E130A suggests this may be a possibility. Additionally, a network of interactions originating from this region of the protein are crucial to native function.

Sequence alignment between KirBac1.1 and other Kir channels is shown in Figure 6. Many residues examined above are partially or completely conserved, implying relevance to hKir channels (Figure 6B−D). Q92 and D115 are not conserved in other channels. Since activity upon mutation to alanine was not significantly impacted, the role of Q92 and D115 may not be directly important for channel conductance, but they may act as hinges to accommodate motions of residues in direct allosteric contact. S104 and E106 are almost fully conserved across all channels. E130 is conserved in bacterial but not hKir channels. This position in hKir channels is typically glutamine, which could fulfill many of the same roles if E130 is protonated. V72, 73, and 133 are not perfectly conserved, but this position is always a branched hydrophobic residue in hKir channels. R181 is fully conserved across the Kir channels, highlighting the different modes of activation between channel types. F149 seems to be conserved in bacterial Kir channels, but most residues at this position are isoleucine or methionine in hKir channels. L140, when aligned with the other channels, is typically replaced with phenylalanine, suggesting a preference for larger side chains. The secondary glycine hinge G137 is not as conserved in hKir channels but seems to be more conserved as a bacterial specialty may stress that the importance of smaller hydrophobic residues is more favorable for TM helix motion across channels. In general, sequence alignments presented herein indicate that many of the observations and accompanying rationale we have presented could be widely applicable to hKir channel physiology.

CONCLUSIONS

Previously, we identified a significant number of residues in KirBac1.1 with chemical shift perturbations triggered in response to channel activation. In this work, we have used knowledge of this proposed allosteric network to generate mutant perturbing function of KirBac1.1. These mutants were probed *via* a fluorescence-based functional assay to characterize the impact of mutations on the channel function. Using CGMD simulations, we have thus performed experiments to characterize the effects of mutation not only on channel flux but also on lipid interaction and ensuing dynamics of structural motifs known to be involved in channel activation and function. Analysis of these coarse grain simulations further provided details of residue−residue contacts speculated to carry these allosteric signals throughout the protein. Last, we have used sequence alignment to extrapolate our observations to hKir channels. Thus, our findings provide insight into both KirBac1.1 and hKir channel physiology and allosteric regulation.

ASSOCIATED CONTENT

Supporting Information

The Supporting Information is available free of charge at https://pubs.acs.org/doi/10.1021/acsomega.2c04456.

K^+ flux assay for KirBac1.1 mutants reconstituted in an activating 60:40 POPC/POPG lipid environment; Na^+ flux assay for KirBac1.1 mutants reconstituted in an activating 60:40 POPC/POPG lipid environment; full PyLipID PG average residency time plots ± std. dev from cutoffs of 0.55 and 1.0 nm CGMD simulations color coded by mutant; CONAN correlation of transmembrane and pore helix residues; CONAN correlation analysis of SF residues; CONAN correlation analysis of pore lining and adjacent residues; Gridmat-MD two-dimensional contour plots of bilayer thickness of the last frame of each simulation; average order parameters for oleoyl acyl beads calculated throughout the simulations with the correlation between % flux and average oleoyl acyl bead order parameter throughout CG simulations as mean ± std and color coded; and alignment of KirBac1.1 with various K^+ channels using the secondary structure provided by the 7SWJ PDB file (PDF)

AUTHOR INFORMATION

Corresponding Author

Benjamin J. Wylie − *Department of Chemistry and Biochemistry, Texas Tech University, Lubbock, Texas 79409, United States;* orcid.org/0000-0001-8183-2762; Email: Benjamin.J.Wylie@ttu.edu

Authors

Maryam Yekefallah − *Department of Chemistry and Biochemistry, Texas Tech University, Lubbock, Texas 79409, United States*

Carver A. Rasberry − *Department of Chemistry and Biochemistry, Texas Tech University, Lubbock, Texas 79409, United States*

Evan J. van Aalst − *Department of Chemistry and Biochemistry, Texas Tech University, Lubbock, Texas 79409, United States*

Holley P. Browning − *Department of Chemistry and Biochemistry, Texas Tech University, Lubbock, Texas 79409, United States*

Reza Amani − *Department of Chemistry and Biochemistry, Texas Tech University, Lubbock, Texas 79409, United States*

Derek B. Versteeg − *Department of Chemistry and Biochemistry, Texas Tech University, Lubbock, Texas 79409, United States*

Complete contact information is available at: https://pubs.acs.org/10.1021/acsomega.2c04456

https://doi.org/10.1021/acsomega.2c04456
ACS Omega 2022, 7, 43621−43634

Author Contributions

Conceptualization, M.Y., C.A.R., E.J.v.A, H.P.B., R.A., D.B.V., and B.J.W.; methodology, M.Y., C.A.R., E.J.v.A, H.P.B., and B.J.W.; software, M.Y., C.A.R., E.J.v.A, and B.J.W.; validation, M.Y., C.A.R., E.J.v.A, and B.J.W.; formal analysis, M.Y., C.A.R., E.J.v.A, and B.J.W.; investigation, M.Y., C.A.R., E.J.v.A, and B.J.W.; resources, M.Y., C.A.R., E.J.v.A, and B.J.W.; data curation, M.Y., C.A.R., E.J.v.A, and B.J.W.; writing—original draft preparation, M.Y., C.A.R., E.J.v.A, and B.J.W.; writing—review and editing, M.Y., C.A.R., E.J.v.A, and B.J.W.; visualization, M.Y., C.A.R., E.J.v.A, and B.J.W.; supervision, B.J.W.; project administration, B.J.W.; funding acquisition, B.J.W. All authors have read and agreed to the published version of the manuscript.

Funding

This work was funded by NIH grant R35GM124979 (Maximizing Investigators' Research Award [MIRA] R35) awarded to Dr. Benjamin J. Wylie.

Notes

The authors declare no competing financial interest.

■ ACKNOWLEDGMENTS

We thank Prof. Michael Latham, and Shane Scoggin for plate reader access. We would like to thank the Texas Tech High Performance Computing Center for providing computational time to run simulations and perform PyLipID analysis. We also thank NMRbox: National Center for Biomolecular NMR Data Processing and Analysis, a Biomedical Technology Research Resource (BTRR), which is supported by NIH grant P41GM111135 (NIGMS), for providing a platform for data analysis.

■ REFERENCES

(1) Pipatpolkai, T.; Usher, S.; Stansfeld, P. J.; Ashcroft, F. M. New insights into KATP channel gene mutations and neonatal diabetes mellitus. *Nat. Rev. Endocrinol.* **2020**, *16*, 378−393.

(2) Manis, A. D.; Hodges, M. R.; Staruschenko, A.; Palygin, O. Expression, localization, and functional properties of inwardly rectifying K+channels in the kidney. *Am. J. Physiol. Ren. Physiol.* **2020**, *318*, F332−F337.

(3) Djukic, B.; Casper, K. B.; Philpot, B. D.; Chin, L. S.; McCarthy, K. D. Conditional knock-out of Kir4.1 leads to glial membrane depolarization, inhibition of potassium and glutamate uptake, and enhanced short-term synaptic potentiation. *J. Neurosci.* **2007**, *27*, 11354−11365.

(4) Suzuki, M.; Li, R. A.; Miki, T.; Uemura, H.; Sakamoto, N.; Ohmoto-Sekine, Y.; Tamagawa, M.; Ogura, T.; Seino, S.; Marbán, E.; Nakaya, H. Functional roles of cardiac and vascular ATP-sensitive potassium channels clarified by Kir6.2-knockout mice. *Circ. Res.* **2001**, *88*, 570−577.

(5) Hibino, H.; Inanobe, A.; Furutani, K.; Murakami, S.; Findlay, I.; Kurachi, Y. Inwardly rectifying potassium channels: their structure, function, and physiological roles. *Physiol. Rev.* **2010**, *90*, 291−366.

(6) Nichols, C.; Lopatin, A. Inward rectifier potassium channels. *Annu. Rev. Physiol.* **1997**, *59*, 171−191.

(7) Lopatin, A. N.; Makhina, E. N.; Nichols, C. G. Potassium channel block by cytoplasmic polyamines as the mechanism of intrinsic rectification. *Nature* **1994**, *372*, 366−369.

(8) Fakler, B.; Brändle, U.; Glowatzki, E.; Weidemann, S.; Zenner, H.-P.; Ruppersberg, J. P. Strong voltage-dependent inward rectification of inward rectifier K+ channels is caused by intracellular spermine. *Cell* **1995**, *80*, 149−154.

(9) Pipatpolkai, T.; Corey, R. A.; Proks, P.; Ashcroft, F. M.; Stansfeld, P. J. Evaluating inositol phospholipid interactions with inward rectifier potassium channels and characterising their role in disease. *Commun. Chem.* **2020**, *3*, 147.

(10) Zangerl-Plessl, E.-M.; Qile, M.; Bloothooft, M.; Stary-Weinzinger, A.; van der Heyden, M. A. G. Disease Associated Mutations in KIR Proteins Linked to Aberrant Inward Rectifier Channel Trafficking. *Biomolecules* **2019**, *9*, 650.

(11) Hager, N. A.; McAtee, C. K.; Lesko, M. A.; O'Donnell, A. F. Inwardly Rectifying Potassium Channel Kir2.1 and its "Kir-ious" Regulation by Protein Trafficking and Roles in Development and Disease. *Front. Cell Dev. Biol.* **2021**, *9*, 796136.

(12) Zhao, Y.; Gameiro-Ros, I.; Glaaser, I. W.; Slesinger, P. A. Advances in Targeting GIRK Channels in Disease. *Trends Pharmacol. Sci.* **2021**, *42*, 203−215.

(13) Tinker, A.; Aziz, Q.; Li, Y.; Specterman, M. ATP-Sensitive Potassium Channels and Their Physiological and Pathophysiological Roles. *Compr. Physiol.* **2018**, *8*, 1463−1511.

(14) Kumar, M.; Pattnaik, B. R. Focus on Kir7.1: physiology and channelopathy. *Channels* **2014**, *8*, 488−495.

(15) Cordero-Morales, J. F.; Vásquez, V. How lipids contribute to ion channel function, a fat perspective on direct and indirect interactions. *Curr. Opin. Struct. Biol.* **2018**, *51*, 92−98.

(16) van Aalst, E.; Yekefallah, M.; Mehta, A. K.; Eason, I.; Wylie, B. Codon Harmonization of a Kir3.1-KirBac1.3 Chimera for Structural Study Optimization. *Biomolecules* **2020**, *10*, 430.

(17) Suh, B. C.; Hille, B. Regulation of ion channels by phosphatidylinositol 4,5-bisphosphate. *Curr. Opin. Neurobiol.* **2005**, *15*, 370−378.

(18) Cabanos, C.; Wang, M.; Han, X.; Hansen, S. B. A Soluble Fluorescent Binding Assay Reveals PIP2 Antagonism of TREK-1 Channels. *Cell Rep.* **2017**, *20*, 1287−1294.

(19) Borcik, C. G.; Eason, I. R.; Yekefallah, M.; Amani, R.; Han, R.; Vanderloop, B. H.; Wylie, B. J. A Cholesterol Dimer Stabilizes the Inactivated State of an Inward-Rectifier Potassium Channel. *Angew. Chem. Int. Ed.* **2022**, *61*, No. e202112232.

(20) Duncan, A. L.; Corey, R. A.; Sansom, M. S. P. Defining how multiple lipid species interact with inward rectifier potassium (Kir2) channels. *Proc. Natl. Acad. Sci. U. S. A.* **2020**, *117*, 7803−7813.

(21) Lee, S. J.; Wang, S. Z.; Borschel, W.; Heyman, S.; Gyore, J.; Nichols, C. G. Secondary anionic phospholipid binding site and gating mechanism in Kir2.1 inward rectifier channels. *Nat. Commun.* **2013**, *4*, 2786.

(22) Lee, S. J.; Ren, F. F.; Zangerl-Plessl, E. M.; Heyman, S.; Stary-Weinzinger, A.; Yuan, P.; Nichols, C. G. Structural basis of control of inward rectifier Kir2 channel gating by bulk anionic phospholipids. *J. Gen. Physiol.* **2016**, *148*, 227−237.

(23) Amani, R.; Borcik, C.; Khan, N.; Versteeg, D.; Yekefallah, M.; Do, H.; Coats, H.; Wylie, B. Conformational changes upon gating of KirBac1.1 into an open-activated state revealed by solid-state NMR and functional assays. *Proc. Natl. Acad. Sci. U. S. A.* **2020**, *117*, 2938−2947.

(24) Splitt, H.; Meuser, D.; Borovok, I.; Betzler, M.; Schrempf, H. Pore mutations affecting tetrameric assembly and functioning of the potassium channel KcsA from Streptomyces lividans. *FEBS Lett.* **2000**, *472*, 83−87.

(25) McCoy, J. G.; Cheng, W.; Thompson, A. N.; Nimigean, C. M.; Nichols, C. G. Mechanism for Selectivity-Inactivation Coupling in KcsA Potassium Channels. *Biophys. J.* **2011**, *100*, 565a.

(26) Bhate, M. P.; McDermott, A. E. Protonation state of E71 in KcsA and its role for channel collapse and inactivation. *Proc. Natl. Acad. Sci. U. S. A.* **2012**, *109*, 15265−15270.

(27) Wylie, B.; Bhate, M.; McDermott, A. Transmembrane allosteric coupling of the gates in a potassium channel. *Proc. Natl. Acad. Sci. U.S.A.* **2014**, *111*, 185−190.

(28) Borcik, C. G.; Versteeg, D. B.; Amani, R.; Yekefallah, M.; Khan, N. H.; Wylie, B. J. The Lipid Activation Mechanism of a Transmembrane Potassium Channel. *J. Am. Chem. Soc.* **2020**, *142*, 14102−14116.

(29) Kuo, A.; Gulbis, J. M.; Antcliff, J. F.; Rahman, T.; Lowe, E. D.; Zimmer, J.; Cuthbertson, J.; Ashcroft, F. M.; Ezaki, T.; Doyle, D. A.

https://doi.org/10.1021/acsomega.2c04456
ACS Omega 2022, 7, 43621−43634

Crystal Structure of the Potassium Channel KirBac1.1 in the Closed State. *Science* **2003**, *300*, 1922−1926.
(30) Enkvetchakul, D.; Bhattacharyya, J.; Jeliazkova, I.; Groesbeck, D. K.; Cukras, C. A.; Nichols, C. G. Functional characterization of a prokaryotic Kir channel. *J. Biol. Chem.* **2004**, *279*, 47076−47080.
(31) Cheng, W. W.; Enkvetchakul, D.; Nichols, C. G. KirBac1.1: it's an inward rectifying potassium channel. *J. Gen. Physiol.* **2009**, *133*, 295−305.
(32) Su, Z.; Brown, E. C.; Wang, W.; MacKinnon, R. Novel cell-free high-throughput screening method for pharmacological tools targeting K+ channels. *Proc. Natl. Acad. Sci. U. S. A.* **2016**, *113*, 5748−5753.
(33) de Jong, D. H.; Singh, G.; Bennett, W. F.; Arnarez, C.; Wassenaar, T. A.; Schäfer, L. V.; Periole, X.; Tieleman, D. P.; Marrink, S. J. Improved Parameters for the Martini Coarse-Grained Protein Force Field. *J. Chem. Theory Comput.* **2013**, *9*, 687−697.
(34) Souza, P. C. T.; Alessandri, R.; Barnoud, J.; Thallmair, S.; Faustino, I.; Grünewald, F.; Patmanidis, I.; Abdizadeh, H.; Bruininks, B. M. H.; Wassenaar, T. A.; Kroon, P. C.; Melcr, J.; Nieto, V.; Corradi, V.; Khan, H. M.; Domański, J.; Javanainen, M.; Martinez-Seara, H.; Reuter, N.; Best, R. B.; Vattulainen, I.; Monticelli, L.; Periole, X.; Tieleman, D. P.; de Vries, A. H.; Marrink, S. J. Martini 3: a general purpose force field for coarse-grained molecular dynamics. *Nat. Methods* **2021**, *18*, 382−388.
(35) Souza, P. C. T.; Thallmair, S.; Conflitti, P.; Ramírez-Palacios, C.; Alessandri, R.; Raniolo, S.; Limongelli, V.; Marrink, S. J. Protein-ligand binding with the coarse-grained Martini model. *Nat. Commun.* **2020**, *11*, 3714.
(36) Pluhackova, K.; Gahbauer, S.; Kranz, F.; Wassenaar, T. A.; Böckmann, R. A. Dynamic Cholesterol-Conditioned Dimerization of the G Protein Coupled Chemokine Receptor Type 4. *PLoS Comput. Biol.* **2016**, *12*, No. e1005169.
(37) Pluhackova, K.; Wilhelm, F. M.; Müller, D. J. Lipids and Phosphorylation Conjointly Modulate Complex Formation of *β*. *Front. Cell Dev. Biol.* **2021**, *9*, 807913.
(38) Gahbauer, S.; Pluhackova, K.; Böckmann, R. A. Closely related, yet unique: Distinct homo- and heterodimerization patterns of G protein coupled chemokine receptors and their fine-tuning by cholesterol. *PLoS Comput. Biol.* **2018**, *14*, No. e1006062.
(39) Khan, A.; Zia, T.; Suleman, M.; Khan, T.; Ali, S. S.; Abbasi, A. A.; Mohammad, A.; Wei, D. Q. Higher infectivity of the SARS-CoV-2 new variants is associated with K417N/T, E484K, and N501Y mutants: An insight from structural data. *J. Cell. Physiol.* **2021**, *236*, 7045−7057.
(40) Khan, A.; Waris, H.; Rafique, M.; Suleman, M.; Mohammad, A.; Ali, S. S.; Khan, T.; Waheed, Y.; Liao, C.; Wei, D. Q. The Omicron (B.1.1.529) variant of SARS-CoV-2 binds to the hACE2 receptor more strongly and escapes the antibody response: Insights from structural and simulation data. *Int. J. Biol. Macromol.* **2022**, *200*, 438−448.
(41) van Aalst, E.; Koneri, J.; Wylie, B. In Silico Identification of Cholesterol Binding Motifs in the Chemokine Receptor CCR3. *Membranes* **2021**, *11*, 570.
(42) Ansell, T. B.; Song, W.; Sansom, M. S. P. The Glycosphingolipid GM3 Modulates Conformational Dynamics of the Glucagon Receptor. *Biophys. J.* **2020**, *119*, 300−313.
(43) Uusitalo, J. J.; Ingólfsson, H. I.; Marrink, S. J.; Faustino, I. Martini Coarse-Grained Force Field: Extension to RNA. *Biophys. J.* **2017**, *113*, 246−256.
(44) Parchekani, J.; Allahverdi, A.; Taghdir, M.; Naderi-Manesh, H. Design and simulation of the liposomal model by using a coarse-grained molecular dynamics approach towards drug delivery goals. *Sci. Rep.* **2022**, *12*, 2371.
(45) Gu, R. X.; Liu, L. A.; Wei, D. Q.; Du, J. G.; Liu, L.; Liu, H. Free energy calculations on the two drug binding sites in the M2 proton channel. *J. Am. Chem. Soc.* **2011**, *133*, 10817−10825.
(46) Hou, S.; Gu, R. X.; Wei, D. Q. Inhibition of *β*-Amyloid Channels with a Drug Candidate wgx-50 Revealed by Molecular Dynamics Simulations. *J. Chem. Inf. Model.* **2017**, *57*, 2811−2821.
(47) Song, W.; Corey, R. A.; Ansell, T. B.; Cassidy, C. K.; Horrell, M. R.; Duncan, A. L.; Stansfeld, P. J.; Sansom, M. S. P. PyLipID: A Python Package for Analysis of Protein-Lipid Interactions from Molecular Dynamics Simulations. *J. Chem. Theory Comput.* **2022**, *18*, 1188−1201.
(48) Mercadante, D.; Gräter, F.; Daday, C. CONAN: A Tool to Decode Dynamical Information from Molecular Interaction Maps. *Biophys. J.* **2018**, *114*, 1267−1273.
(49) Wang, S. Z.; Alimi, Y.; Tong, A.; Nichols, C. G.; Enkvetchakul, D. Stabilization of KirBac1.1 Tetramer by Blocking Ions. *Biophys. J.* **2009**, *96*, 467a.
(50) Borcik, C. G.; Versteeg, D. B.; Wylie, B. J. An Inward-Rectifier Potassium Channel Coordinates the Properties of Biologically Derived Membranes. *Biophys. J.* **2019**, *116*, 1701−1718.
(51) Amani, R.; Schwieters, C. D.; Borcik, C. G.; Eason, I. R.; Han, R.; Harding, B. D.; Wylie, B. J. Water Accessibility Refinement of the Extended Structure of KirBac1.1 in the Closed State. *Front. Mol. Biosci.* **2021**, *8*, 772855.
(52) Lomize, M. A.; Pogozheva, I. D.; Joo, H.; Mosberg, H. I.; Lomize, A. L. OPM database and PPM web server: resources for positioning of proteins in membranes. *Nucleic Acids Res.* **2012**, *40*, D370−D376.
(53) Lee, J.; Cheng, X.; Swails, J. M.; Yeom, M. S.; Eastman, P. K.; Lemkul, J. A.; Wei, S.; Buckner, J.; Jeong, J. C.; Qi, Y.; Jo, S.; Pande, V. S.; Case, D. A.; Brooks, C. L., 3rd; MacKerell, A. D., Jr.; Klauda, J. B.; Im, W. CHARMM-GUI Input Generator for NAMD, GROMACS, AMBER, OpenMM, and CHARMM/OpenMM Simulations Using the CHARMM36 Additive Force Field. *J. Chem. Theory Comput.* **2016**, *12*, 405−413.
(54) Jo, S.; Kim, T.; Iyer, V. G.; Im, W. CHARMM-GUI: a web-based graphical user interface for CHARMM. *J. Comput. Chem.* **2008**, *29*, 1859−1865.
(55) Qi, Y.; Ingólfsson, H. I.; Cheng, X.; Lee, J.; Marrink, S. J.; Im, W. CHARMM-GUI Martini Maker for Coarse-Grained Simulations with the Martini Force Field. *J. Chem. Theory Comput.* **2015**, *11*, 4486−4494.
(56) Hsu, P. C.; Bruininks, B. M. H.; Jefferies, D.; Cesar Telles de Souza, P.; Lee, J.; Patel, D. S.; Marrink, S. J.; Qi, Y.; Khalid, S.; Im, W. CHARMM-GUI Martini Maker for modeling and simulation of complex bacterial membranes with lipopolysaccharides. *J. Comput. Chem.* **2017**, *38*, 2354−2363.
(57) Monticelli, L.; Kandasamy, S. K.; Periole, X.; Larson, R. G.; Tieleman, D. P.; Marrink, S. J. The MARTINI Coarse-Grained Force Field: Extension to Proteins. *J. Chem. Theory Comput.* **2008**, *4*, 819−834.
(58) Periole, X.; Cavalli, M.; Marrink, S. J.; Ceruso, M. A. Combining an Elastic Network With a Coarse-Grained Molecular Force Field: Structure, Dynamics, and Intermolecular Recognition. *J. Chem. Theory Comput.* **2009**, *5*, 2531−2543.
(59) Berendsen, H. J. C.; Postma, J. P. M.; van Gunsteren, W. F.; DiNola, A.; Haak, J. R. Molecular Dynamics with Coupling to an External Bath. *J. Chem. Phys.* **1984**, *81*, 3684−3690.
(60) Allen, W. J.; Lemkul, J. A.; Bevan, D. R. GridMAT-MD: a grid-based membrane analysis tool for use with molecular dynamics. *J. Comput. Chem.* **2009**, *30*, 1952−1958.
(61) Maciejewski, M. W.; Schuyler, A. D.; Gryk, M. R.; Moraru, I. I.; Romero, P. R.; Ulrich, E. L.; Eghbalnia, H. R.; Livny, M.; Delaglio, F.; Hoch, J. C. NMRbox: A Resource for Biomolecular NMR Computation. *Biophys. J.* **2017**, *112*, 1529−1534.
(62) Madeira, F.; Park, Y. M.; Lee, J.; Buso, N.; Gur, T.; Madhusoodanan, N.; Basutkar, P.; Tivey, A. R. N.; Potter, S. C.; Finn, R. D.; Lopez, R. The EMBL-EBI search and sequence analysis tools APIs in 2019. *Nucleic Acids Res.* **2019**, *47*, W636−W641.
(63) Robert, X.; Gouet, P. Deciphering key features in protein structures with the new ENDscript server. *Nucleic Acids Res.* **2014**, *42*, W320−W324.
(64) Matamoros, M.; Nichols, C. Pore-forming transmembrane domains control ion selectivity and selectivity filter conformation in

https://doi.org/10.1021/acsomega.2c04456
ACS Omega 2022, 7, 43621−43634

the KirBac1.1 potassium channel. *J. Gen. Physiol.* **2021**, *153*, No. e202012683.
(65) Domene, C.; Grottesi, A.; Sansom, M. S. Filter flexibility and distortion in a bacterial inward rectifier K+ channel: simulation studies of KirBac1.1. *Biophys. J.* **2004**, *87*, 256−267.
(66) Linder, T.; Wang, S. Z.; Zangerl-Plessl, E. M.; Nichols, C. G.; Stary-Weinzinger, A. Molecular Dynamics Simulations of KirBac1.1 Mutants Reveal Global Gating Changes of Kir Channels. *J. Chem. Inf. Model.* **2015**, *55*, 814−822.

https://doi.org/10.1021/acsomega.2c04456
ACS Omega 2022, 7, 43621−43634